WIND TUNNEL TEST AND AERODYNAMIC ANALYSIS OF THREE AEROELASTICALLY TAILORED WINGS+

W. W. Braymen*
W. A. Rogers*

General Dynamics, Fort Worth Division
Fort Worth, Texas

M. H. Shirk**

AFWAL, Flight Dynamics Laboratory
Wright-Patterson AFB, Ohio

ABSTRACT

Aeroelastic tailoring of composite lifting surfaces was validated in a program that involved design, fabrication, and transonic wind tunnel testing of three static aeroelastic wings in addition to a set of steel wings. Each aeroelastic wing had unique design objectives. The test featured aeroelastic shape documentation through the use of photogrammetry along with the simultaneous acquisition of forces and pressures. Highlights of the aerodynamic test results are presented, with emphasis placed on test-to-theory comparisons. The strong points as well as areas of needed improvement in the aerodynamic design methods are discussed. The investigation demonstrates that the design of composite lifting surfaces should include consideration of aerodynamic benefits available through tailoring.

INTRODUCTION

In the design of a high-performance fighter aircraft, the aerodynamicist has inevitably been faced with the problem of compromise in order to configure the vehicle to best meet performance requirements over a wide range of Mach/lift/altitude conditions. Aeroelastic tailoring of a composite wing box can reduce this compromise considerably by providing the capability to obtain camber and twist under high-load maneuver conditions without paying the camber/twist drag penalty at cruise and acceleration conditions. The unique feature of aeroelastic tailoring is that beneficial aeroelastic characteristics, such as increased twist and camber and increased flutter speed, are actively sought and controlled during the design process rather than being the analytical consequence of a design based on strength and flutter considerations alone. This is accomplished by varying the ply orientations and thickness distributions in the composite laminate to establish the structural characteristics that provide the desired response.

General Dynamics, under contract to the Air Force Flight Dynamics Laboratory, developed the Wing Aeroelastic Synthesis Procedure (generally referred to as TSO) to automate the tailoring design process by use of structural optimization methods.[1,2] Under a subsequent contract, an aeroelastic drag analysis capability was added and the code was used to explore potential performance payoffs for fighter and bomber configurations.[3,4] In 1978, a program was initiated to validate the aeroelastic tailoring methods through correlation of the design methods with wind tunnel test data obtained on static aeroelastic and flutter models designed with the methods. An overview of the entire effort was given in an earlier paper.[5] The purpose of the present paper is to present more complete details of the aerodynamic findings of the study, with emphasis on test-to-theory results. The total effort is documented in a final report to the Air Force.[6]

CONFIGURATION SELECTION AND MODEL DESIGN

A 1/9-scale wing/body-of-revolution/strake configuration was selected for the study. The configuration is shown in Figure 1, which illustrates the wind tunnel model

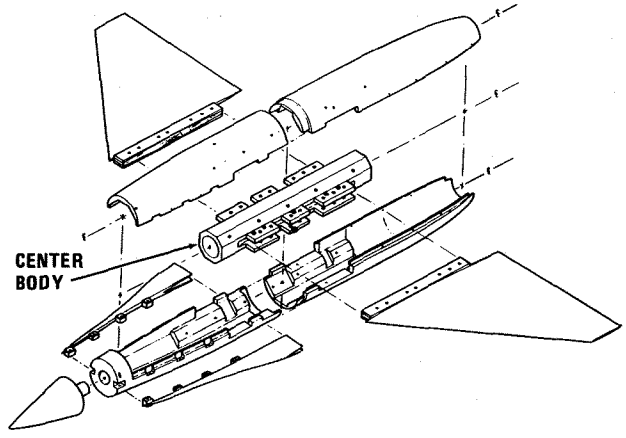

• WING	FULL SCALE
AREA	338.29 Ft^2
SPAN	399.726 In.
THEO ROOT CHORD	200.738 In.
MAC, $\bar{c}$	138.882 In.
ASPECT RATIO	3.28
TAPER RATIO	0.2142
SWEEP	40.0°
AIRFOIL	NACA 64A004 @ Tip NACA 64A003.5 @ Root
INCIDENCE	0°
TWIST	0°
• FUSELAGE	
OVERALL LENGTH	547.000 In.
MAX BODY DIA	55.400 In.

Figure 1 Selected Wing/Body/Strake Configuration

+ This research was sponsored by the Air Force Wright Aeronautical Laboratories, Flight Dynamics Laboratory, Wright-Patterson AFB, Ohio.

* Engineering Specialist, Member AIAA.

** Prinicpal Scientist, Analysis and Optimization Branch, Structures and Dynamics Division, Member AIAA.

as it was eventually designed and fabricated. The wing planform evolved from an Independent Research and Development program to maximize transonic maneuverability without sacrificing good supersonic characteristics.[7] The wing had been tested previously on a blended wing/body/strake configuration. In addition, it was quite similar to a wing that showed aeroelastic tailoring potential during a previous study.[3] No camber or twist was included in the undeformed jig shape.

Three sets of aeroelastic model wings were designed with the TSO procedure to duplicate the flexible characteristics of corresponding full-scale wings. Aerodynamic loads for TSO were provided by the linear-theory panel-method of Carmichael.[8] Each set of wings had a unique design objective, and duplication of the full-scale aeroelastic camber and twist in the model wings was a primary consideration. The objective of one design was to maximize transonic maneuver through aeroelastic camber and negative or washout twist. The objective of the second design was to demonstrate increased lift-curve slope through attainment of aeroelastic camber and positive or washin twist (potential application to vertical tail design for increased effectiveness). In order to provide a measure of the aerodynamic gains resulting from aeroelastic tailoring, the third set of wings was not tailored for aerodynamic reasons but, instead, was typical of traditional composite lifting surfaces.

The ply orientations of the wings are summarized in Figure 2. The nontailored wing had ply orientations of 0°, +45°, and -45°, where the plus and minus 45° plies were

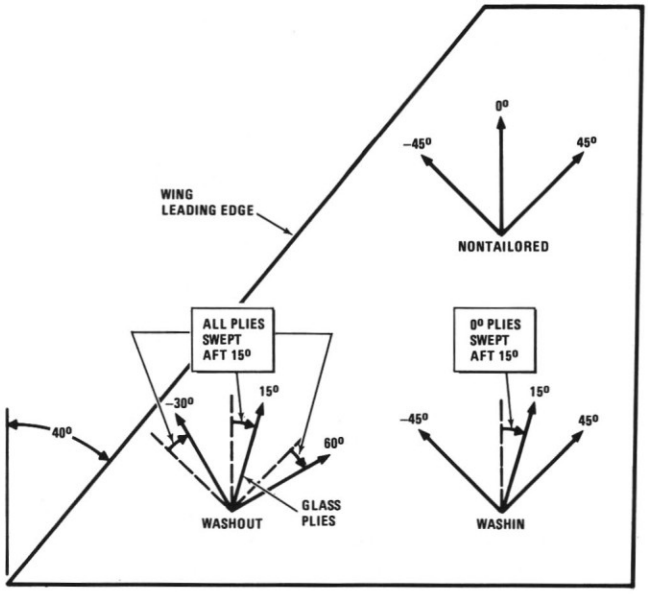

Figure 2 Ply Orientations for Aeroelastic Designs

balanced, occurring in equal amounts. The washout wing had all three ply orientations rotated aft 15°; furthermore, the wing was an unbalanced hybrid laminate with graphite epoxy crossplies (+60° and -30°) and unidirectional glass at +15°. The full-scale washin wing contained no glass plies but had the spanwise plies rotated aft 15°. All of the model wings required use of unidirectional glass-epoxy in addition to graphite-epoxy in order to duplicate full-scale flexibilty while providing enough strength to withstand proof-loading to twice the expected wind tunnel test loads.

Since the wind tunnel tests were to be conducted at the Arnold Engineering Development Center (AEDC) PWT-16T wind tunnel, a dynamic pressure of 750 lb/ft^2 was selected to simulate the full-scale flight condition of Mach 1.2 at 10,000 feet of altitude (dynamic pressure = 1467 psf) in order to remain within the tunnel capability. The resulting model scale factor for dynamic pressure was 750/1467 = 0.511.

MODEL FABRICATION AND INSTRUMENTATION

The fuselage components and strake were machined from 7075 aluminum, whereas the centerbody and rigid wings were machined from 4340 steel. The aeroelastic wings were fabricated from glass-graphite-epoxy laminates and Nomex^R core. Left-hand and right-hand steel female tools were fabricated for the lay-up and cure of the laminates. The steel molds provided close control of the wing external geometry. The skin laminates were cured at elevated temperature and pressure in a cavity press.

The following types of instrumentation were included in the model:

1. An internal six-component balance.

2. Ninety-eight static pressure orifices located on the upper and lower wing surfaces. Upper-surface pressures were measured on the right wing panel, and lower surface pressures were measured on the left panel. Additional pressure taps were located in the fuselage, two near the balance and two near the exit, to measure base drag.

   Complete pressure distributions were obtained on the aeroelastic wings, but only one row of five orifices was located on the upper-surface leading edge of the rigid wing to provide a measure of leading-edge separation.

3. Photographic targets located on the wings and fuselage to allow determination of wing deflection through application of photogrammetry.[9] Briefly, the technique provides complete instantaneous documentation of the model shape by securing a simultaneous pair of photographs of the model from two viewpoints in the ceiling of the wind tunnel by use of stroboscopic lighting. Optical targets consisting of a white dot on a contrasting dark background were positioned on the wing as shown in Figure 3. Reference coordinates of these targets and similar reference targets placed on the fuselage were obtained from pre-test model inspections and from analysis of air-off photographs obtained during the wind tunnel tests. A system of equations established through data reduction of each stereo pair is solved to yield the location of each target in three dimensions with a relative uncertainty of ±.006 inch between any two targets on the wing.

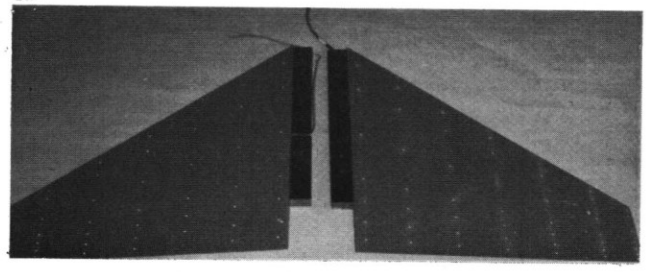

Figure 3 Steel Wing With Optical Targets

4. Foil strain gages located on the upper and lower surfaces of the left wing panel and on the centerbody tabs to provide steady-state and dynamic measurements of bending moment. These gages and an additional semiconductor gage located on the upper left wing panel also provided data for analysis of buffet characteristics.

LABORATORY TESTS

The aeroelastic wings underwent detailed laboratory tests prior to wind tunnel testing. Each panel was proof-loaded to 1000 pounds using a whiffle-tree fixture to distribute the load. Influence coefficients were obtained at 25 locations using photogrammetry to establish the model deformation. Ground vibration tests were conducted on each set of wings, by softly supporting the complete model, including centerbody, from springs and testing the configuration as a free-free model. Laboratory tests were also conducted to determine the model's vibration characteristics when installed on the wind tunnel test sting and balance.

WIND TUNNEL TEST

The 1/9-scale model, shown in Figure 4, was tested in the AEDC PWT-16T wind tunnel from September 28 to October 5, 1979. Data were obtained at Mach numbers from 0.6 to 1.2 at dynamic pressures that produced

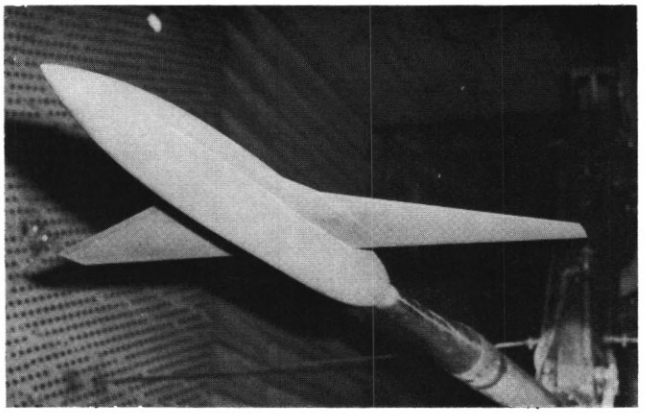

Figure 4 Model Installed in AEDC PWT-16T Wind Tunnel

aeroelastic responses corresponding to altitudes from sea level to 30,000 feet. The nominal test Reynolds numbers and dynamic pressures are summarized in Table 1. Testing was accomplished at angles of attack from -10 degrees to +28 degrees with limits dependent on Mach number and dynamic pressure. High-angle-of-attack directional stability data were obtained from -10 degrees to +10 degrees of sideslip for selected Mach-number/altitude conditions.

Total forces, pressures, photogrammetry data, and steady-state and dynamic bending moments were recorded simultaneously. Oil flow photographs as well as motion pictures were obtained at selected conditions. Documentation of the aeroelastic shape was recorded for 165 Mach-number/dynamic-pressure/angle-of-attack conditions.

The initial part of the test was conducted with the rigid wing to answer several questions. A brief grit-size study was accomplished to determine if it would be

Table 1 WIND TUNNEL TEST VALUES OF REYNOLDS NUMBER AND DYNAMIC PRESSURE

SIMULATED ALTITUDE	MACH NUMBER					
	0.60	0.85	0.90	0.95	1.10	1.20
	REYNOLDS NUMBER/FT (x 10^{-6})					
SEA LEVEL	2.1	–	3.5	–	–	–
10,000 FEET	1.5	2.2	2.4	2.6	3.2	3.7
30,000 FEET	–	–	1.0	–	–	1.6
	DYNAMIC PRESSURE (PSF)					
SEA LEVEL	273	–	613	–	–	–
10,000 FEET	187	376	422	470	630	750
30,000 FEET	–	–	182	–	–	323

necessary to change grit size as Reynolds number was varied. The results showed that grit No. 100 could be used to ensure a turbulent boundary layer at the lower Reynolds numbers and not produce separated flow at the higher Reynolds numbers. Therefore, this one grit size was utilized for the remainder of the test.

A second question addressed with the rigid wing was whether Reynolds number changes had a significant effect on the aerodynamic characteristics, particularly drag due to lift. Although the rigid wing showed a slight reduction in drag due to lift with increasing Reynolds number because of its small amount of aeroelasticity, the results confirmed that the thin wing was not producing significant Reynolds number effects that could mask the evaluation of the aeroelastic wings.

The final question of concern was whether the use of the body-of-revolution fuselage might result in adverse interference effects on the wing. As mentioned previously, rigid-model test data on a blended wing/body/strake of identical wing planform were available from an earlier test. Comparison of these blended-body data with the data obtained on the body-of-revolution fuselage confirmed that the simplified fuselage was producing results that correlated quite closely with the blended configuration.

The rigid wing was also tested upright and inverted to establish flow angularity corrections. Complete testing of the rigid and three aeroelastic wings was then accomplished. Each of the wings, including the rigid wing, was tested at the same Mach/dynamic-pressure conditions to provide for direct comparison of results.

Each of the wings was tested with the strake. The rigid and washout wings were also tested without the strake.

WIND TUNNEL TEST HIGHLIGHTS

The drag characteristics of the three aeroelastic wings in addition to those for the rigid wing are shown in Figure 5 at the design condition of Mach 0.9 and 10,000 feet of altitude. The washout wing achieved its objective of reduced maneuver drag by demonstrating a 23% reduction in drag due to lift at the design lift coefficient of 0.7 (9-g load factor). At the same condition, the nontailored wing produced a 7% reduction. Data reduction of the photogrammetry results confirmed that the washout wing was achieving the desired results through a combination of aeroelastic twist and camber. The drag-due-to-lift increment at Mach 0.9 between the

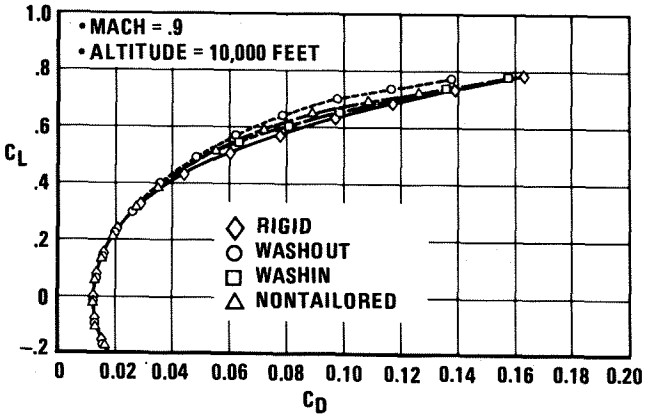

Figure 5 Drag Comparison of Aeroelastic Wings and Rigid Wing at the Design Condition

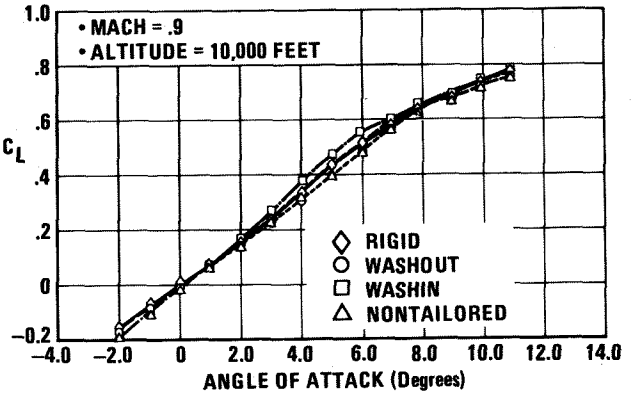

Figure 7 Lift Comparison of Aeroelastic Wings and Rigid Wing at the Design Condition

washout and rigid wings is shown in Figure 6 for sea-level, 10,000 feet, and 30,000 feet of altitude. Significant drag reduction was demonstrated even at 30,000 feet. The higher dynamic pressure required to simulate the sea-level condition restricted the maximum lift coefficient at which data could be obtained.

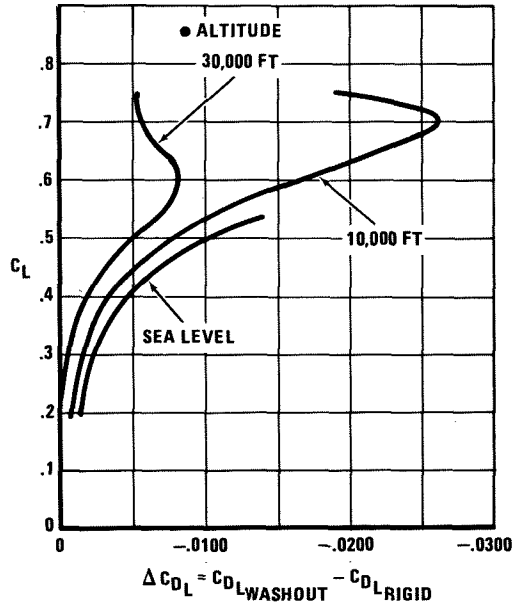

Figure 6 Altitude Effects on Drag at Mach 0.9 for Washout Wing

The lift-curve results at the design condition for the four wings, shown in Figure 7, reveal that the washin wing also achieved its objective of providing increased lift-curve slope. A 16% increase in lift-curve slope was achieved for the washin wing compared to the rigid wing in the angle-of-attack range between -2 and +4 degrees. Although photogrammetry revealed that the nontailored wing was producing washout twist, it too was cambering sufficiently to yield a 5% increase in lift-curve slope. A summary of the washin wing test lift-curve slopes is provided in Figure 8 as a function of Mach number and altitude. The increase in lift effectiveness compared to the rigid wing is significant at all Mach numbers except Mach 1.1 and 1.2, which showed a slight decrease.

The chordwise pressure distributions, shown in Figure 9 at the design condition, confirm the favorable drag results of the washout wing. (As mentioned earlier, rigid wing pressures were measured only near the leading

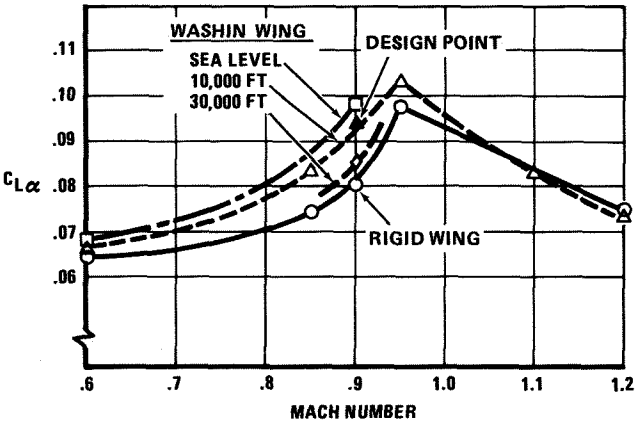

Figure 8 Washin Wing Lift-Curve-Slope Characteristics

edge.) All of the wings show attached flow inboard at span station A (η = 0.45), indicated by the large negative upper-surface leading-edge pressure peak and the strong pressure recovery approaching the trailing edge. The washout wing retains the strong leading-edge pressure peak at all span stations shown, and the results show evidence of trailing-edge separation only near the tip (η = 0.89). However, both leading- and trailing-edge separation are evident for the other three wings at all span stations shown except the most inboard. For these wings, the leading-edge pressure peak and chordwise pressure recovery deteriorates across the span.

The importance of aeroelastic twist and camber is further illustrated in Figure 10, which compares pressures at the outboard station at a lift coefficient of approximately 0.55 (Mach 0.9, 10,000 feet of altitude). At this reduced lift coefficient, the nontailored wing is twisting and cambering sufficiently to retain attached flow on the upper surface while the rigid and washin wing results still indicate separated flow. However, as shown in Figure 11, when the lift coeffficient is increased to approximately 0.78, even the washout wing upper-surface flow is no longer attached.

Pitching moment results, presented in Figure 12, correspond to the lift and drag results shown in Figures 5 and 7. Although all of the aeroelastic wings show an aft aerodynamic center (a.c.) shift compared to the rigid wing, the washout wing achieves the highest lift coefficient before an unstable break, which occurs at the design lift coefficient. Additional tests with a horizontal

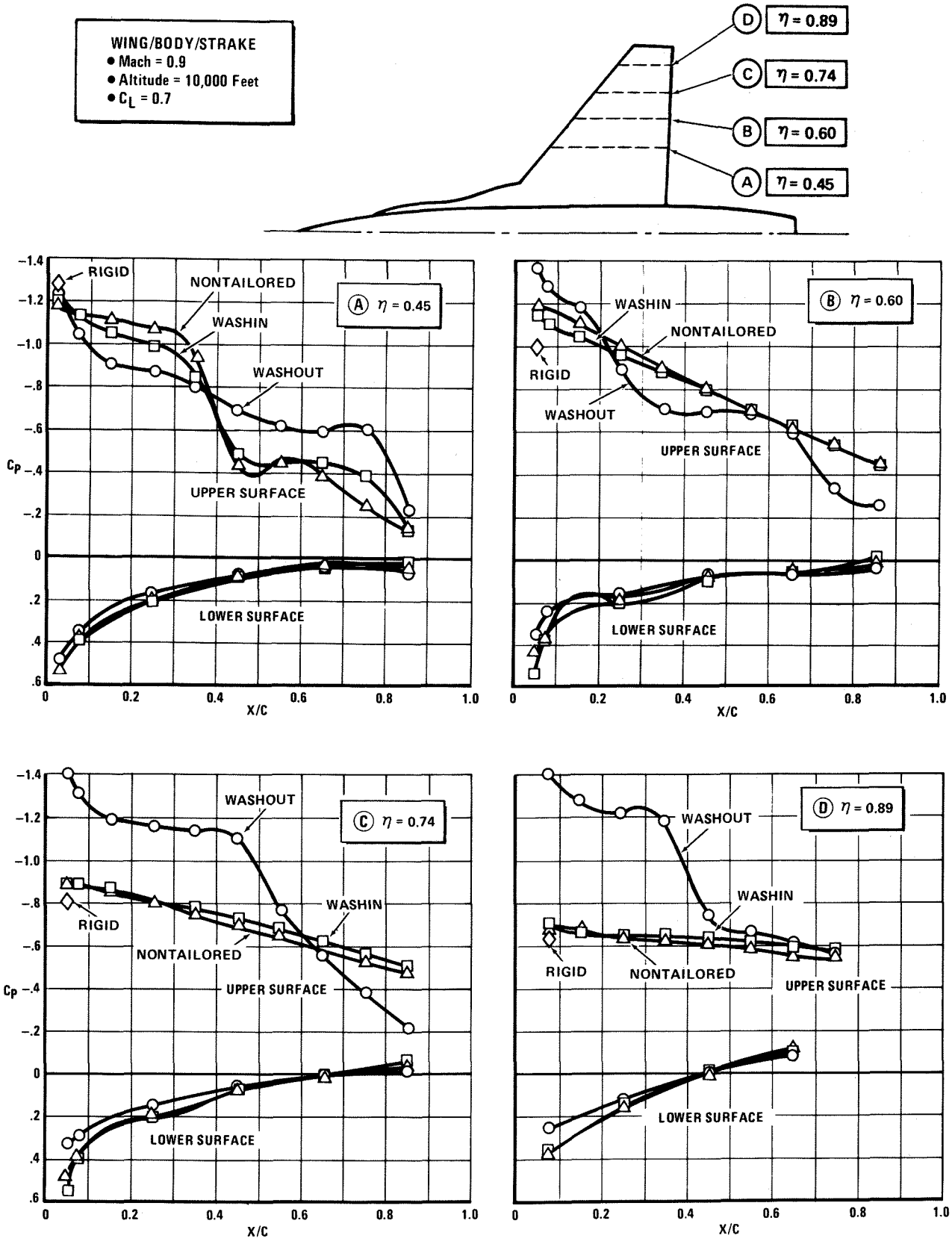

Figure 9 Comparison of Pressure Distributions at the Design Condition

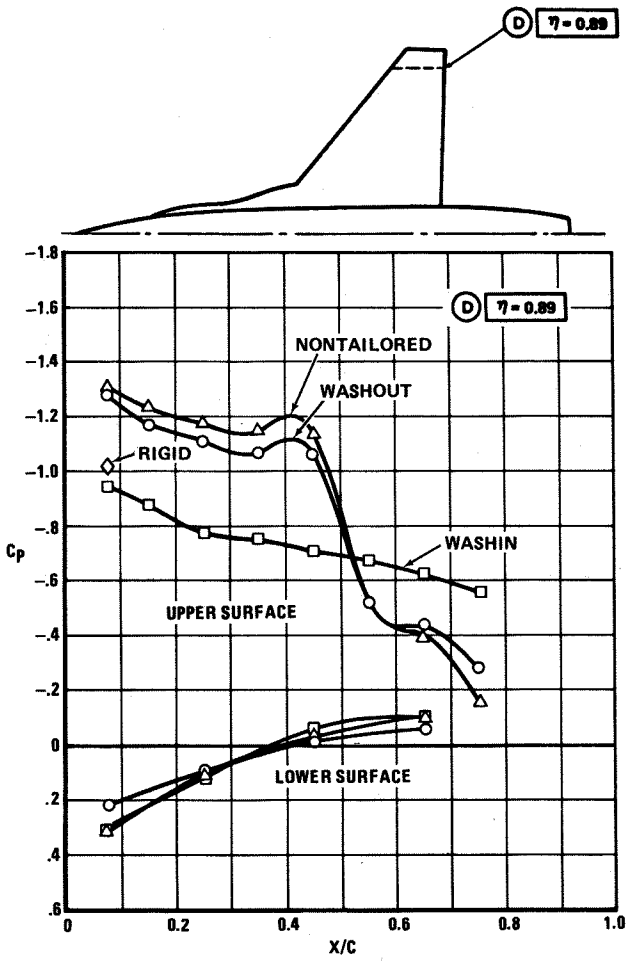

Figure 10 Comparison of Outboard Wing Pressures at Mach = 0.9, Altitude = 10,000 Feet, $C_L \approx 0.55$

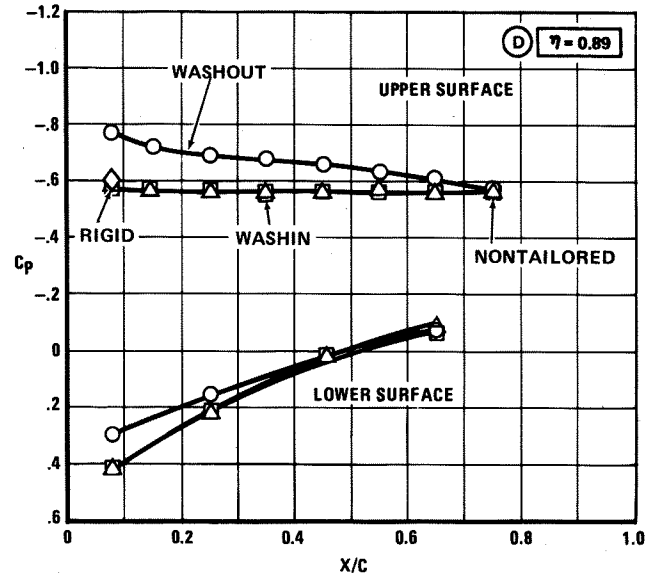

Figure 11 Comparison of Outboard Wing Pressures at Mach = 0.9, Altitude = 10,000 Feet, $C_L \approx 0.78$

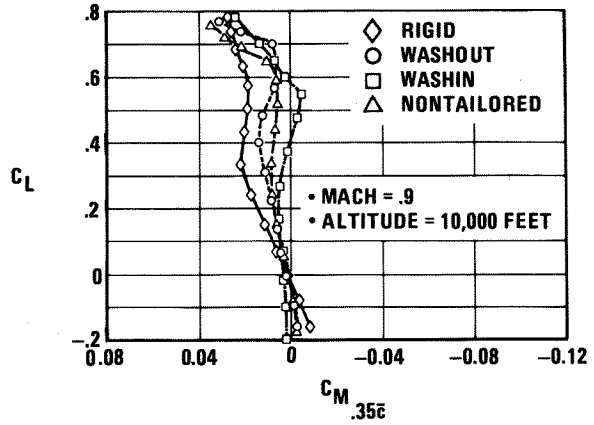

Figure 12 Pitching Moment Comparison of Aeroelastic Wings and Rigid Wing at the Design Condition

tail would be required to establish if the unstable break is a significant problem. Figure 13 shows that the washout wing produces a forward shift in a.c. supersonically to combine with the aft shift subsonically to yield a net reduction in subsonic-to-supersonic a.c. travel. Aeroelastic tailoring could thus be used to reduce supersonic trim drag. However, it is noted in the earlier paper[5], that the washout wing does not produce any improvement in the untrimmed drag at Mach 1.2 compared to the rigid wing.

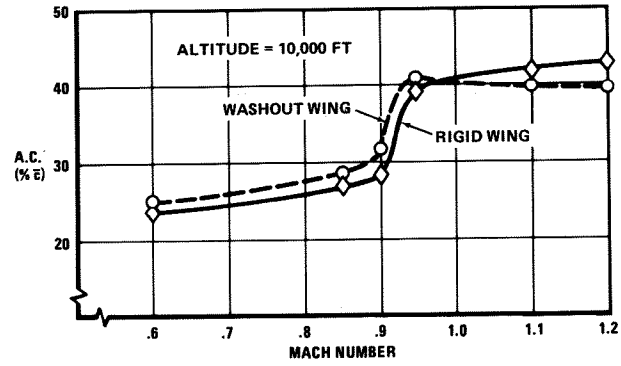

Figure 13 Comparison of Aerodynamic Center Characteristics for Washout and Rigid Wings

TEST-TO-THEORY COMPARISONS

Analyses of the wind tunnel data established that the design objectives were demonstrated and that the quality of the data was very good. The force data, pressure data, and photogrammetric results were consistent and provided a good data set for test-to-theory correlations.

The acquisition of both in-tunnel aeroelastic geometry and wing pressures allowed for an independent evaluation of both the aerodynamic and structural methodology used in TSO. This was accomplished in the following way. To evaluate the structural simulation, the measured pressure distributions were used to provide loads for input to TSO, from which aeroelastic shapes were calculated for comparison with the photogrammetric results. Similarly, to evaluate the aerodynamic simulation, the measured in-tunnel shapes were used to predict aerodynamic characteristics for correlation with

test forces and pressures. This paper deals only with the aerodynamic correlations.

The correlations were accomplished by the following three approaches:

1. Carmichael[8] linear theory with aeroelastic characteristics based on the TSO structural simulation. This provided an assessment of the overall TSO aerodynamic/structural representation.

2. Carmichael linear theory based on aeroelastic geometry as determined from in-tunnel photogrammetry results. Comparison of these results with the test data provided an evaluation of the aerodynamic method used in the design of the wings.

3. Bailey-Ballhaus[10] transonic finite-difference nonconservative solutions based on aeroelastic geometry as determined from the photogrammetry results used in (2) above. Comparison of these results with test data and with the predictions obtained in (2) provided an assessment of linear theory with a nonlinear transonic code.

The panel arrangement shown in Figure 14 was used in the Carmichael test-to-theory analyses as well as in the design of the models. It required 186 panels to model the wing, strake, and fuselage. (Comparison of wing pressures obtained with this fuselage modeling approach showed insignificant differences with those obtained where the body was simulated as an isolated body in combination with wing-body interference panels.[6]) However, it is noted that, whereas the Carmichael simulations included the fuselage and strake, the Bailey-Ballhaus analyses represented only the theoretical wing (to the centerline). This approach was selected on the basis of test-to-theory correlations made in an earlier study.[11] Those results revealed that the highly swept strake produced a mathematically unacceptable skewed mesh arrangement. The study also showed the nonconservative wing-alone solutions to correlate better with test data than the conservative, wing-body solutions and at least as good with conservative, viscous wing-body solutions.

The Bailey-Ballhaus code iteratively solves a modified form of the small-disturbance equation which retains higher-order terms to improve resolution of swept shocks. The computational domain is defined by use of an embedded mesh approach. A Cartesian crude grid discretizes the entire computational domain, while a planform-oriented fine mesh discretizes the region of the flow field around the wing.

Test-to-theory comparisons of total forces are presented in Figure 15 for the washout wing at the design condition of Mach 0.9 and 10,000 feet of altitude. The lift characteristics are shown in Figure 15(a); also shown are the aeroelastic increments obtained by subtracting the rigid wing results (not shown) from the flexible wing results at constant values of lift coefficient. The calculations dependent on photogrammetry data are shown only at lift coefficients of 0.57 and 0.70. The results reveal that all three approaches underestimate the lift; however, use of the tunnel-derived wing shapes shows somewhat better correlation, with Bailey-Ballhaus being the best. The vortex lift produced by the strake is not accounted for in either the Carmichael or Bailey-Ballhaus formulation, which explains at least in part the lower analytical results.

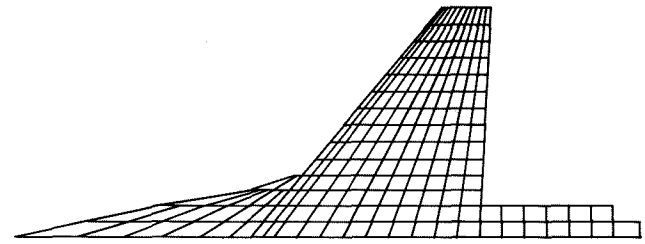

Figure 14 Paneling Arrangement Used in Linear Theory Analyses

Correlations of pitching moment are shown in Figure 15(b). As with the lift results, the aeroelastic increment in pitching moment obtained between the washout and rigid wings at constant lift coefficient is shown. Correlation of pitching moment is clearly the best for the Bailey-Ballhaus approach. This is as expected, since the technique can predict shock effects, which shift the a.c. aft. The aeroelastic moment increments calculated with the Carmichael and Bailey-Ballhaus approaches are comparable.

Drag-due-to-lift correlations are presented in Figure 15(c). The Carmichael results (using both TSO predictions and photogrammetric geometry) include empirical adjustments to account for the effect of partial leading-edge suction below the polar break and to determine an estimate of the polar-break lift coefficient.[3,4] These factors were established prior to the wind tunnel test based on test data obtained on the blended wing-body configuration mentioned earlier. The correlations of drag due to lift and the aeroelastic increment between the washout and rigid wings are better for the Carmichael results, with the use of photogrammetric data providing slightly improved results. The Bailey-Ballhaus results are not as good, but it is noted that no empirical adjustments were made to the results.

Test-to-theory comparisons of washout wing pressure distributions are presented in Figure 16(a) at the design lift coefficient of 0.7 for Mach 0.9, 10,000 feet of altitude. Prediction of pressures at a lift coefficient of 0.7 represents a challenge for both linear theory and transonic finite-difference techniques, but it is a realistic and practical design condition. Although six chordwise rows of test pressures were obtained, data for only the outboard three stations are included here to show correlations where the aeroelastic effects are the largest. The TSO/Carmichael and Carmichael (with test geometry) results show only slight differences. Since these calculations employ linear theory, no shock effects are predicted. Both the upper- and lower-surface pressures are more positive than the test data. The net chordwise loading is also underpredicted at the two most outboard span stations. The Bailey-Ballhaus approach shows considerably better correlation in this complex flow regime. The leading-edge pressures agree very well, and the general characteristics of the flow are modeled, particularly for $\eta = 0.60$. However, the pressure jump across the shock is progressively overpredicted as the tip is approached, resulting in a negative loading for the most outboard station shown. The discrepancy at the tip station is also increased as a result of trailing-edge separation, illustrated in the test data by the loss of pressure recovery aft of the shock. The separated flow causes the shock location to move forward.

Since trailing-edge separation was apparent for the lift coefficient of 0.7, similar correlations were made at a lift coefficient of 0.57, as shown in Figure 16(b). Also, results are included that were obtained by using the

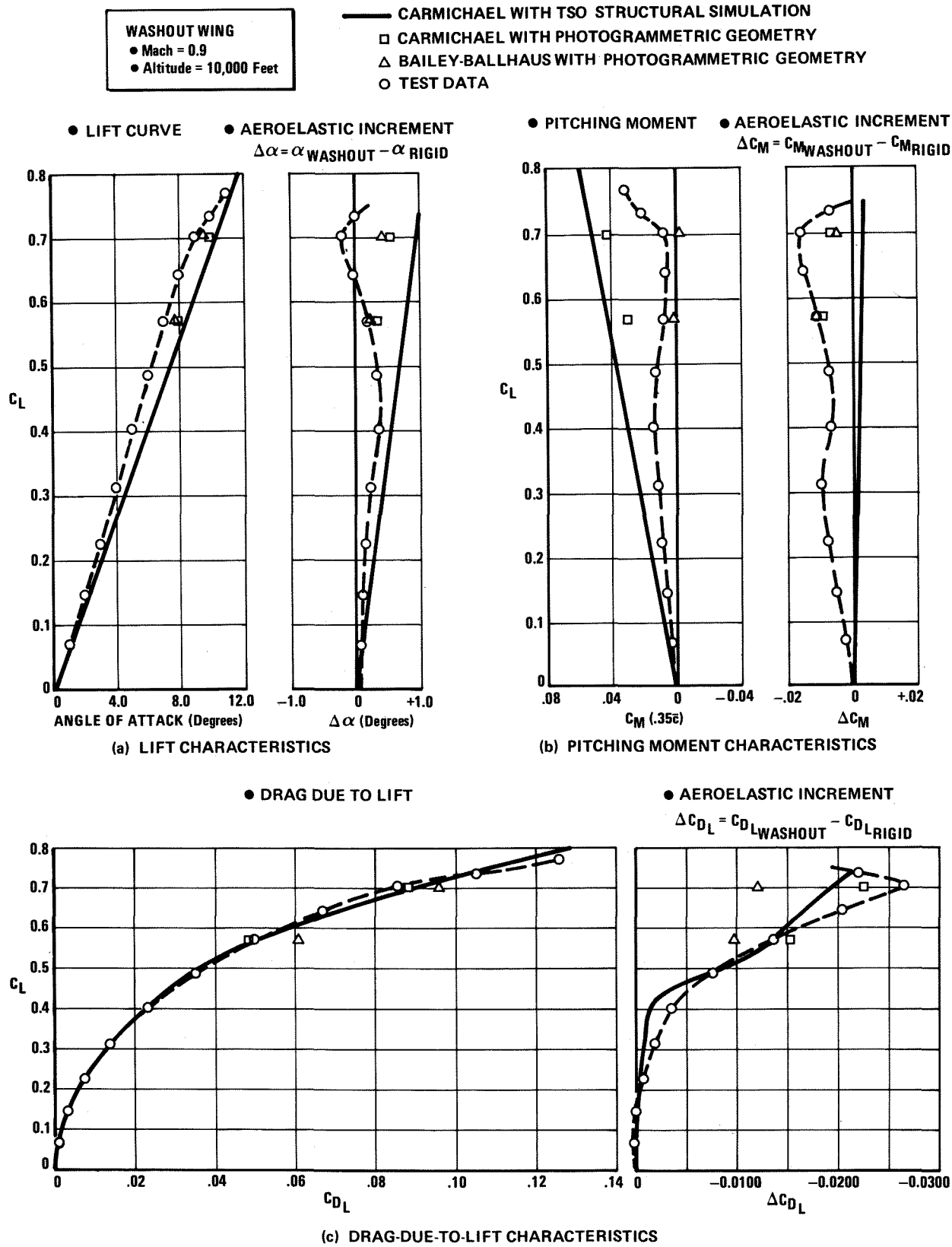

Figure 15 Test-to-Theory Correlations of Total Forces for Washout Wing at the Design Condition

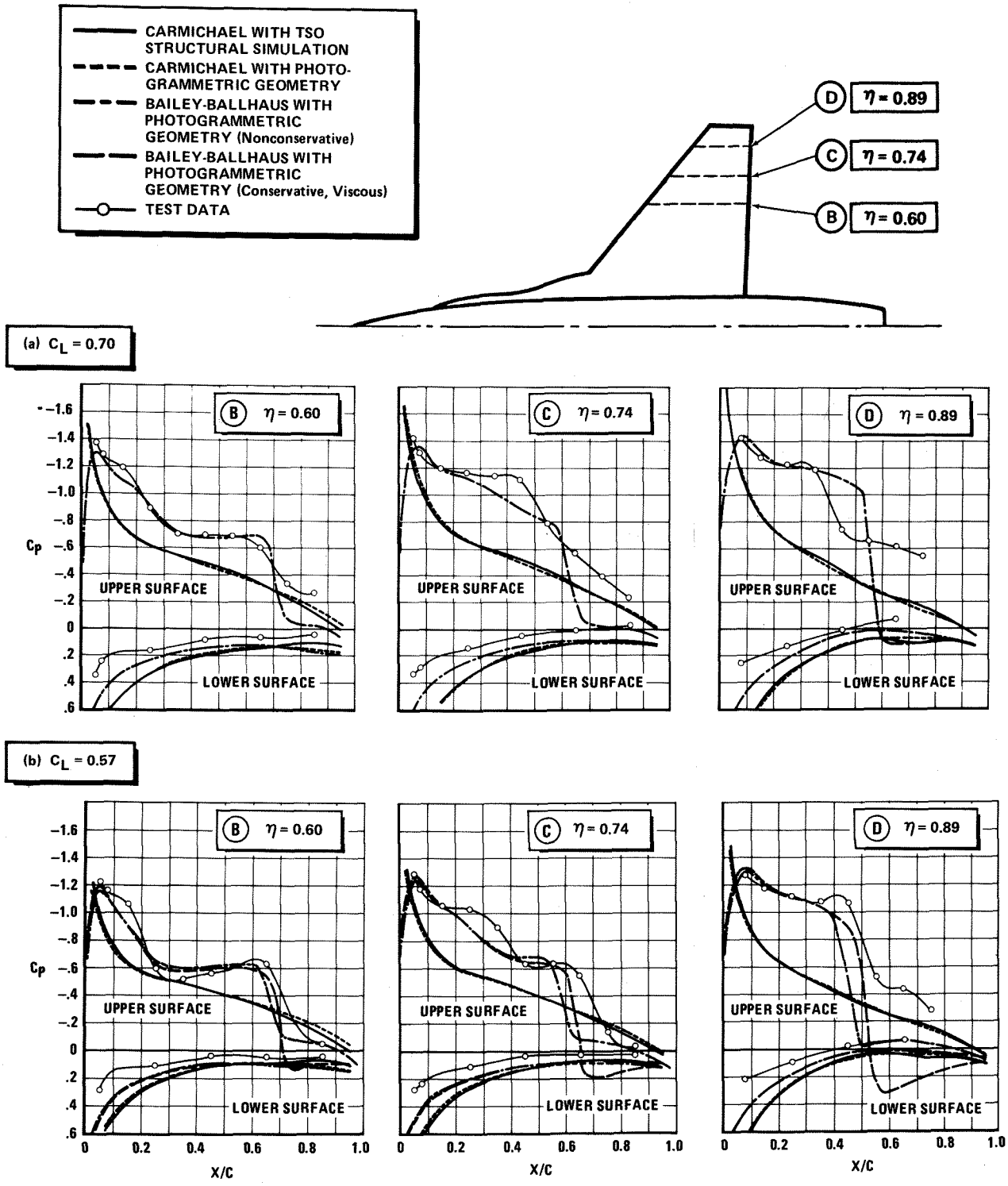

Figure 16 Pressure Distribution Correlations for Washout Wing at Mach = 0.9, Altitude = 10,000 Feet

conservative, viscous option in the Bailey-Ballhaus code. Although the conservative, viscous option provides some improvement in predicted shock location, the shock strength is much too high. The nonconservative Bailey-Ballhaus results provide reasonably good correlation, with one exception. The predicted shock location is too far forward, even at the tip. The predicted shock strengths actually correlate quite well except for the most outboard station. It was observed that shock strength was good when the local Mach number ahead of the shock was approximately 1.25 or less. Comparison of the linear theory results with the test data reveal similar differences to those noted in Figure 15(a).

Linear theory results compare much better with test data at Mach 1.2 than at Mach 0.9, as would be expected. Though not shown here, the total forces predicted with linear theory correlated better than those obtained with the Bailey-Ballhaus code. This probably reflects the better geometrical modeling used in the linear theory calculations (wing/body/strake versus wing only). Test-to-theory comparisons of washout wing pressure

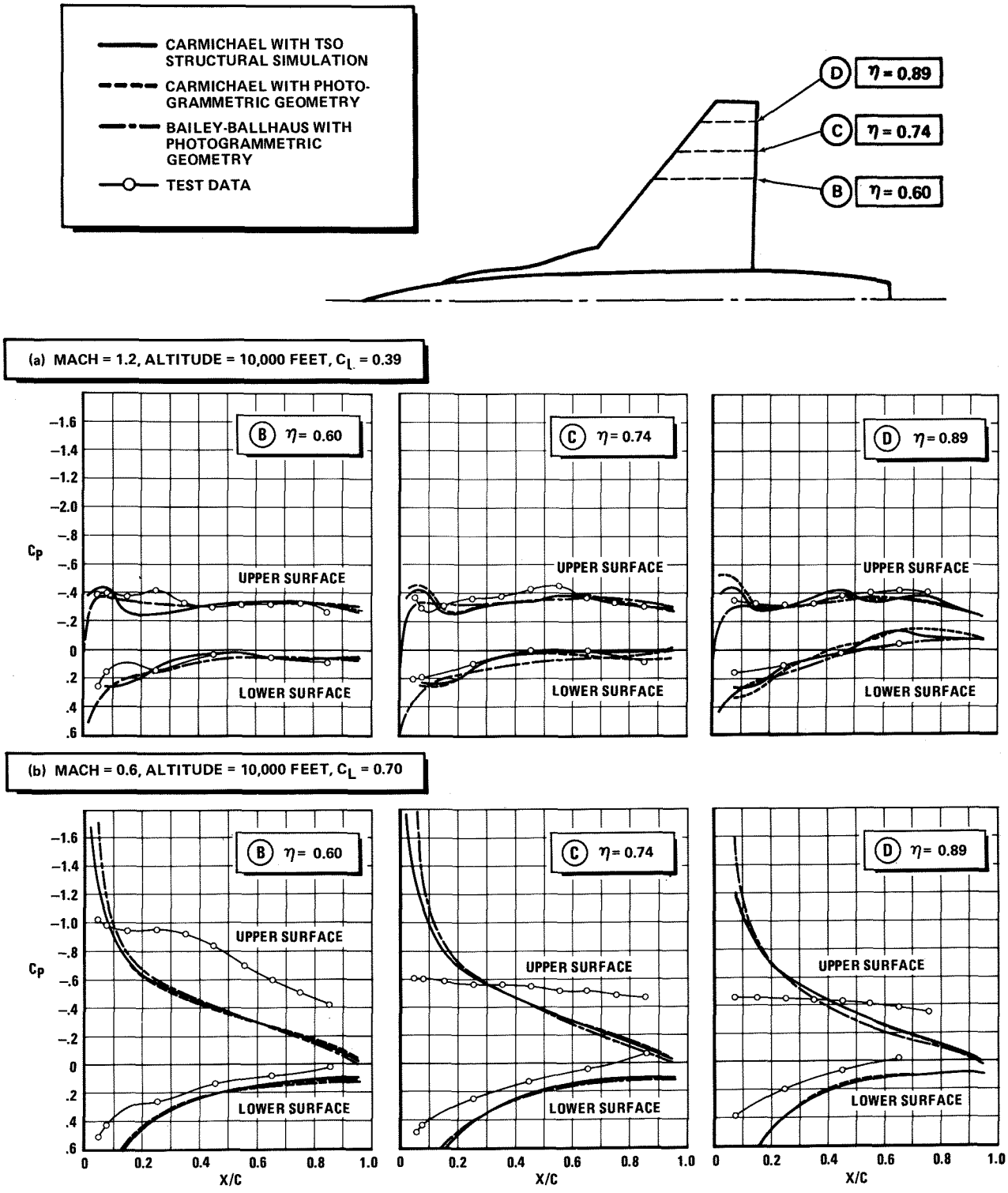

Figure 17 Pressure Distribution Correlations for Washout Wing at Off-Design Mach Numbers

distributions at Mach 1.2, 10,000 feet of altitude, and lift coefficient of 0.39 (load factor = 9 g) are shown in Figure 17(a). Each of the analytical approaches produces essentially comparable results with one exception. The Bailey-Ballhaus results provide better agreement in net loading in the leading-edge region. Linear theory produces leading-edge pressure peak loads that are too large.

Pressure distribution correlations are shown in Figure 17(b) for the washout wing at Mach 0.6, 10,000 feet of altitude, and 0.7 lift coefficient. The test data correspond to an angle of attack of greater than 11 degrees and reveal completely separated flow characteristics. The dynamic pressure is simply too low at this condition to produce enough aeroelastic response to keep the flow attached. Since none of the analytical approaches account for separated flow, the correlations are very poor.

Span load distributions, shown in Figure 18, correspond to the pressure data presented in Figures 16(a)

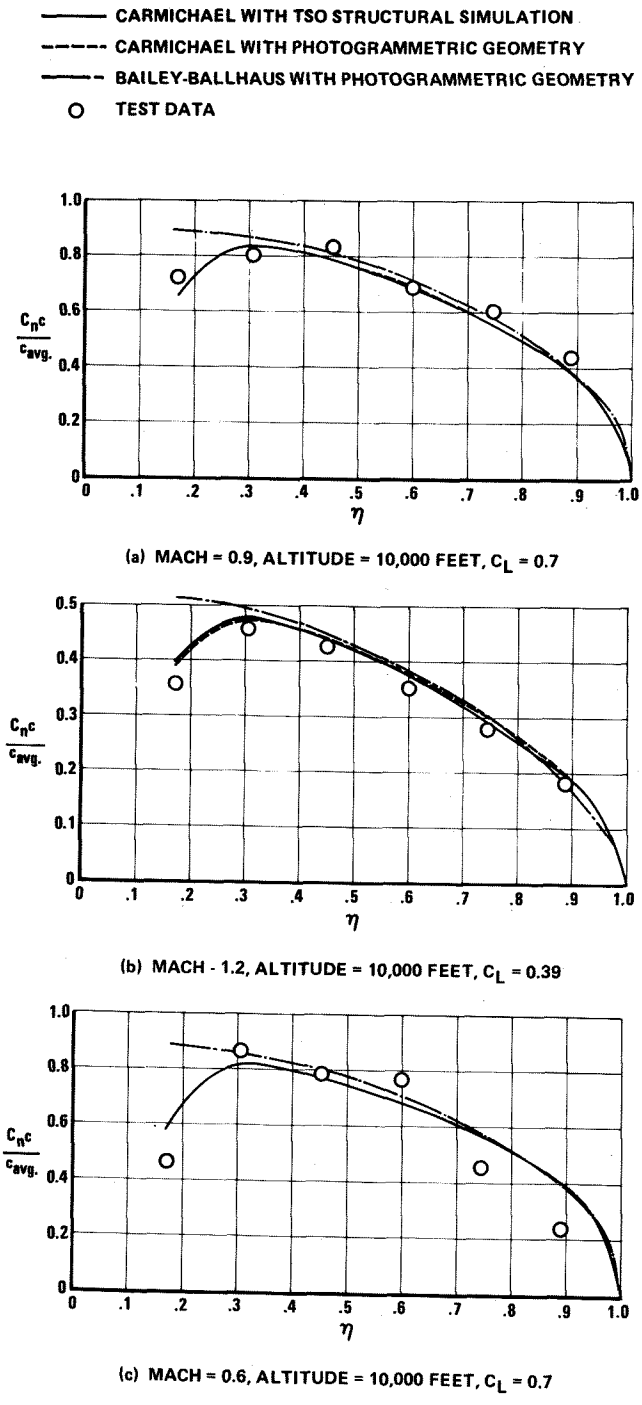

Figure 18 Spanwise Load Distribution Correlations for Washout Wing

and 17. At the most inboard station, the drop in loading is due to the strake being located ahead of the wing and the strake loads not being included in either the test data or the linear theory results. However, the Bailey-Ballhaus simulation did not model the strake and therefore does not show a decrease in loading. The test-to-theory comparisons are very good at the Mach 0.9 and 1.2 conditions. It is noteworthy that while significant differences existed in the pressure distributions at Mach 0.9 between the Carmichael and Bailey-Ballhaus calculations, the corresponding span load distributions are comparable. At Mach 0.6 the separated-flow problem discussed above resulted in poor correlation at the outboard stations on the wing.

The test-to-theory comparisons presented to this point have been shown for the washout wing. The correlations of total forces for the washin and nontailored wings are similar to those obtained for the washout wing. However, the pressure distribution correlations for the washin and nontailored wings are generally poorer because of the large regions of separated flow on the outboard portion of the wings. This point is illustrated in Figure 19, which shows pressure distributions at one span station for the washin and nontailored wings (Mach 0.9, 10,000 feet of altitude, lift coefficient of 0.7). The extent of the separated flow is revealed in the loss of leading-edge suction and poor chordwise pressure recovery characteristics. The strong viscous effects result in unacceptable correlation by any of the three theoretical approaches. Although the nonconservative Bailey-Ballhaus case tends to simulate a pseudo-viscous solution, it by no means accounts for separated flow.

Span load distributions for the washin and nontailored wings, shown in Figure 20, correspond to the pressure data in Figure 19. The loss in lift on the outboard portion of the wings caused by the separated flow results in overprediction of the span load. This contrasts to the washout wing results shown in Figure 18(a), where the test loads are actually higher than the predicted loads near the tip.

CONCLUSIONS

The wind tunnel test results obtained in this program have successfully demonstrated the concept of aeroelastic tailoring. The washout wing produced significant reduction in transonic drag due to lift and the washin wing achieved increased lift-curve slope due to aeroelastic tailoring. This technology provides the designer with an additional tool to achieve his objectives.

Although the TSO/Carmichael procedure has demonstrated its effectiveness in preliminary design of aeroelastically tailored wings, the test-to-theory correlations show obvious areas of needed improvement. The problems basically stem from the fact that aeroelastic tailoring shows the greatest payoffs at transonic high-angle-of-attack conditions; unfortunately, this is the Mach and lift regime for which aerodynamic

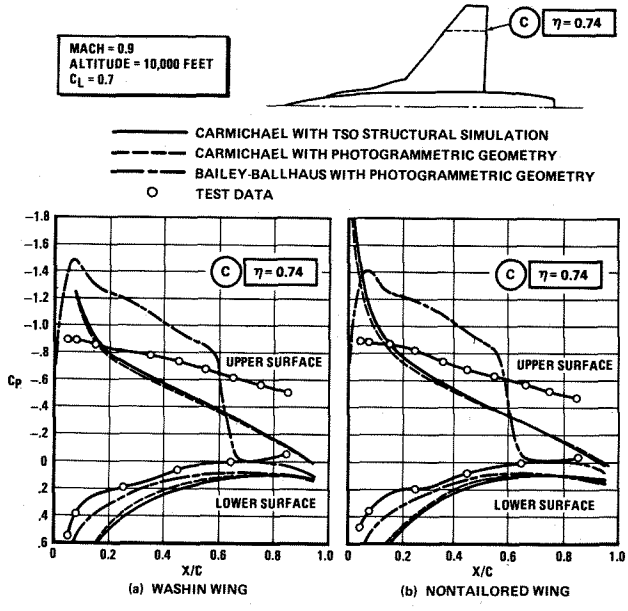

Figure 19 Pressure Distribution Correlations for Wasbin and Nontailored Wings

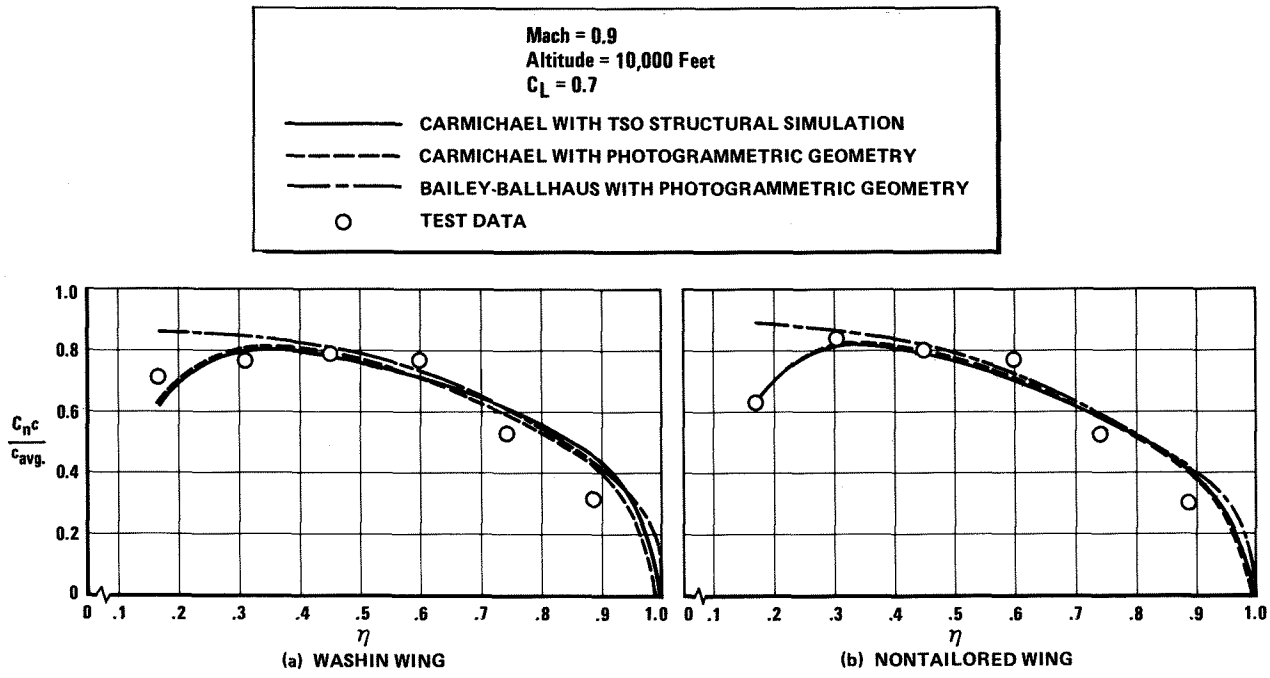

Figure 20 Spanwise Load Distribution Correlations for Washin and Nontailored Wings at the Design Condition

characteristics are most difficult to predict. Transonic high-angle-of-attack conditions press both linear theory and the current transonic codes to practical limits.

The principal advantage of linear theory in an iterative design procedure such as TSO lies in its speed. Also, reasonably complex geometries (such as highly swept strakes) can be represented. Linear theory can provide good predictions of chordwise and spanwise loads at subsonic and supersonic speeds if the flow is attached. However, the mixed flow present at transonic speeds and separated flow conditions are not handled. Also, linear theory requires the use of empirical factors to account for partial leading-edge suction in the prediction of drag characteristics.

The strength of the Bailey-Ballhaus procedure is its ability to account for mixed flow conditions, including prediction of transonic shocks. It was observed that the predicted shock strength was quite good for conditions where the local Mach number ahead of the shock was 1.25 or less, although the shock location was not necessarily correct. Unfortunately, the local Mach number exceeded this value on the outboard portion of the wings at the design condition, resulting in shock strengths that were too high and predicted shock locations that were ahead of the test data. As with linear theory, separated flow is not handled. The transonic codes are somewhat restrictive in geometry simulation; in particular, problems were encountered in attempting to model the highly swept strake. At present the nonlinear transonic codes are impractical for use in TSO because of the large number of iterations required to obtain a solution. The Bailey-Ballhaus solutions obtained in this program required as many as 1700 iterations and 54 minutes of CDC 7600 CP time. Development of transonic aerodynamic codes that are suitable for use with a preliminary design procedure such as TSO should be encouraged.

REFERENCES

1. McCullers, L. A. and Lynch, R. W., "Composite Wing Design for Aeroelastic Tailoring Requirements," presented at the Air Force Conference on Fibrous Composites in Flight Vehicle Design, Dayton, Ohio, 26-28 September 1972.

2. McCullers, L. A. and Lynch, R. W., Dynamic Characteristics of Advanced Filamentary Composite Structures, AFFDL-TR-73-111, Volume II, Air Force Flight Dynamics Laboratory, Wright-Patterson Air Force Base, Ohio, September 1974.

3. Lynch, R. W., Rogers, W. A., and Braymen, W. W., Aeroelastic Tailoring of Advanced Composite Structures for Military Aircraft, AFFDL-TR-76-100, Volumes I through III, Air Force Flight Dynamics Laboratory, Wright-Patterson Air Force Base, Ohio, February 1978.

4. Lynch, R. W., Rogers, W. A., and Braymen, W. W., "An Integrated Capability for the Preliminary Design of Aeroelastically Tailored Wings," AIAA Paper No. 76-912, September 1976.

5. Rogers, W. A., Braymen, W. W., and Shirk, M. H., "Design, Analyses, and Model Tests of an Aeroelastically Tailored Lifting Surface," AIAA Paper No. 81-1673, August 1981.

6. Rogers, W. A., Braymen, W. W., Murphy, A. C., Graham, D. H., and Love, M. H., Validation of Aeroelastic Tailoring by Static Aeroelastic and Flutter Tests, AFWAL-TR-81-3160, Air Force Wright Aeronautical Laboratories, Wright-Patterson Air Force Base, Ohio.

7. Lydick, L. N. and Mann, H. W., Status Report on Development of a Variable Contour Wing Design for Fighter Aircraft, General Dynamics Report ERR-FW- 1653, December 1975.

8. Carmichael, R. L., Castellano, C. R., and Chen, F. C., The Use of Finite Element Methods for Predicting the Aerodynamics of Wing-Body Combinations, NASA SP- 228, October 1969.

9. Brooks, J. D. and Beamish, J. K., "Measurement of Model Aeroelastic Deformations in the Wind Tunnel at Transonic Speeds Using Stereophotogrammetry," NASA Technical Paper 1010, 1977.

10. Ballhaus, W. F., Bailey, F. R., and Frick, J., "Improved Computational Treatment of Transonic Flow About Swept Wings," Advances in Engineering Science, Volume 4, NASA CP-2001, 1976, pp. 1311-1320.

11. Bhateley, I. C., Mann, M. J., and Ballhaus, W. F., "Evaluation of Three-Dimensional Transonic Methods for the Analysis of Fighter Configurations," AIAA Paper No. 79-1528, July 1979.